Hindawi
Advances in Meteorology
Volume 2019, Article ID 1545746, 14 pages
https://doi.org/10.1155/2019/1545746

Research Article

Projected Effects of Climate Change on Future Hydrological Regimes in the Upper Yangtze River Basin, China

Yuqian Wang,[1] Xiaoli Yang,[1,2] Mengru Zhang,[1] Linqi Zhang,[1] Xiaohan Yu,[1] Liliang Ren,[1,2] Yi Liu,[1,2] Shanhu Jiang,[1,2] and Fei Yuan[1,2]

[1]*College of Hydrology and Water Resources, Hohai University, Nanjing 210098, China*
[2]*State Key Laboratory of Hydrology-Water Resources and Hydraulic Engineering, Hohai University, Nanjing 210098, China*

Correspondence should be addressed to Xiaoli Yang; yangxl@hhu.edu.cn

Received 18 August 2018; Revised 27 October 2018; Accepted 9 December 2018; Published 14 January 2019

Academic Editor: Margarida L. R. Liberato

Climate change directly impacts the hydrological cycle via increasing temperatures and seasonal precipitation shifts, which are variable at local scales. The water resources of the Upper Yangtze River Basin (UYRB) account for almost 40% and 15% of all water resources used in the Yangtze Basin and China, respectively. Future climate change and the possible responses of surface runoff in this region are urgent issues for China's water security and sustainable socioeconomic development. This study evaluated the potential impacts of future climate change on the hydrological regimes (high flow (Q_5), low flow (Q_{95}), and mean annual runoff (MAR)) of the UYRB using global climate models (GCMs) and a variable infiltration capacity (VIC) model. We used the eight bias-corrected GCM outputs from Phase 5 of the Coupled Model Intercomparison Project (CMIP5) to examine the effects of climate change under two future representative concentration pathways (RCP4.5 and RCP8.5). The direct variance method was adopted to analyze the contributions of precipitation and temperature to future Q_5, Q_{95}, and MAR. The results showed that the equidistant cumulative distribution function (EDCDF) can considerably reduce biases in the temperature and precipitation fields of CMIP5 models and that the EDCDF captured the extreme values and spatial pattern of the climate fields. Relative to the baseline period (1961–1990), precipitation is projected to slightly increase in the future, while temperature is projected to considerably increase. Furthermore, Q_5, Q_{95}, and MAR are projected to decrease. The projected decreases in the median value of Q_{95} were 21.08% to 24.88% and 16.05% to 26.70% under RCP4.5 and RCP8.5, respectively; these decreases were larger than those of MAR and Q_5. Temperature increases accounted for more than 99% of the projected changes, whereas precipitation had limited projected effects on Q_{95} and MAR. These results indicate the drought risk over the UYRB will increase considerably in the future.

1. Introduction

The Yangtze is one of the longest rivers in the world, and the area surrounding this river is among the most developed, dynamic, densely populated, and highly concentrated industrial areas in China [1–3]. Meanwhile, the Yangtze River Basin (YRB) is the main water resource of the South-to-North Water Transfer Project, and it is dominated by two types of monsoon current flow in a year: the Siberian northwest winter monsoon and the Asian southeast summer monsoon. These two weather patterns are extraordinarily vulnerable to climate change due to their large seasonal and interannual variabilities in precipitation and temperature. In recent decades, the frequencies of floods and droughts in the YRB have been higher than elsewhere in China, which has led to much heavier socioeconomic losses [4–8]. For example, the great flood of 1998 inundated 213,106 hectares (21 Mha) of land and destroyed five million houses in the YRB, causing an economic loss of over US$20 billion [5]. Earth system models from Phase 5 of the Coupled Model Intercomparison Project (CMIP5) projected a warming trend of 0.47°C/10 years and 0.73°C/10 years over China in the 21st century under emission scenarios representative concentration pathways RCP4.5 and RCP8.5, respectively [9]. These projected climate changes may cause more natural droughts and floods, especially when coupled with local

precipitation and temperature changes in this region. Additionally, population and economic growth will result in an increased demand for water for drinking and industrial activities. Therefore, understanding the potential impacts of future climate change on the river discharge of the YRB has become an increasingly urgent issue of water security and is essential for assisting policymakers in adopting strategies to address extreme events.

Several previous studies have estimated the hydrological change response to climate change over the YRB. Xiao et al. [10] analyzed the intra-annual variations, tendencies, and mutational sites of runoff during the historical period in the YRB. Gu et al. [11] found that the runoff in the northern part of the Yangtze River will increase by approximately 10% from 2070 to 2099 due to climate change according to RegCM4.0 of the SRES A1B scenario. Qian et al. [12] considered terrestrial water storage changes within the YRB using the variable infiltration capacity (VIC) model under the SRES A2 and B2 climate scenarios. Koirala et al. [13] considered the runoff from 11 CMIP5 models together with a routing model and found that little change will occur in the discharge from the YRB due to the increased projected precipitation. Su et al. [9] used the VIC model and 20 CMIP5 global climate models (GCMs) and found that the total runoff is projected to increase by 10.7–21.4% during 2041–2070 under RCP8.5. Birkinshaw et al. [1] found that the projected changes in the basin's annual discharge range from −29.8 to +16.0% from 2041 to 2070 based on the results of 35 GCM models under RCP8.5. However, a large number of studies have focused on the monthly and annual mean discharges or the timings of the monthly mean discharge change during different climate scenarios rather than on the extreme discharge in the future. As reported by the IPCC [14], the increasing numbers of floods and droughts may both be associated with changes in the extremes of runoff and streamflow, which are more sensitive to climate changes within local regions, especially for large river source regions [13, 15, 16]. The water resources of the UYRB account for almost 40% and 15% of the total water resources of the YRB and the whole of China. Possible changes in high flow and low flow over UYRB represent vital information for future water resource management and water security for the whole YRB. Therefore, in addition to considering the location, topography, and basin storage of the UYRB, projecting the climate change impacts on the spatiotemporal characteristics of hydrological regimes (mean runoff, high flow, and low flow) in the upstream region is more important for local water security.

Hydrological models driven by climate model projections are considered a reliable method for projecting future climate change and assessing its hydrological consequences [17]. Statistical and dynamic downscaling methods are the main bridges spanning the resolution gap between GCMs and hydrological models. In both cases, statistical downscaling methods can identify potential sources of climate model bias and increase confidence in the simulated changes of a surface climate [18–20]. The statistical downscaling method may provide a more appropriate approach than that of dynamical downscaling when station or extreme value points are required or when computational resources are limited [21]. Within statistical downscaling methods, the quantile mapping bias-correction method is the most popular method. This method adjusts the distribution of the model output to match all statistical moments with respect to the observations. Li et al. [22] developed the EDCDF method using an adjusted bias to bias correct historical and projected model simulations, and the method proved to be efficient for reducing model biases by considering future uncertainty in climate fields [23, 24]. Aloysius et al. [25] and Yang et al. [26] proved that the EDCDF method is more efficient when model biases are reduced and can provide more reliable simulations and projections of the future extreme value of climate fields.

Therefore, in this study, one of our main objectives is to validate the performance of the downscaled outputs of eight GCMs (precipitation and temperature) via the EDCDF method [26]. For the same variables, we use the output of eight GCMs under the high and middle representative concentration pathways (RCP4.5 and RCP8.5) for the period from 2006 to 2099. In addition, coupled with the results of the eight bias-corrected CMIP5 models, the VIC model is applied to a $0.5 \times 0.5^{\circ}$ grid cell to simulate the runoff of the whole basin from 1961 to 2099. Three hydrological regimes (mean annual runoff, high flow, and low flow) are selected to evaluate the impacts of climate change under the RCP4.5 and RCP8.5 scenarios. Finally, the contribution of precipitation and temperature to the hydrological regimes is quantified by the direct variance method. In Discussion, the potential effects of climate change on water resources and food security are discussed based on social statistical data. This work provides a comprehensive study in the UYRB to explore the impact of climate changes on future hydrological regimes.

2. Datasets and Methods

2.1. Datasets. Daily observed precipitation and temperature data covering the period of 1961–2005 from 87 stations in the UYRB are provided by the National Climate Center of China Meteorological Administration. The daily discharge (1961–2005) at the Yichang hydrological station was obtained from the Yangtze River Hydrological Bureau of China. The locations of these stations and the digital elevation model (DEM) are shown in Figure 1. During the historical period, all of the stations are in operation and have the same period records of precipitation and temperature. The soil texture of the UYRB is derived from the 5-min Food and Agriculture Organization (FAO) dataset [27]. Vegetation data and their characteristic parameters are based on the 1 km global vegetation dataset developed at the University of Maryland [28]. All data are interpolated to a $0.5 \times 0.5^{\circ}$ grid cell structure.

In this study, the daily precipitation and temperature data from eight GCMs (bcc-csm1-1, CanESM2, CCSM4, CSIRO-Mk3-6-0, GISS-E2-R, MRI-CGCM3, MPI-ESM-LR, and NorESM1-M) participating in CMIP5 are used to project climate changes (Table 1). This study uses only the results from the most extreme RCP8.5 and moderate RCP4.5

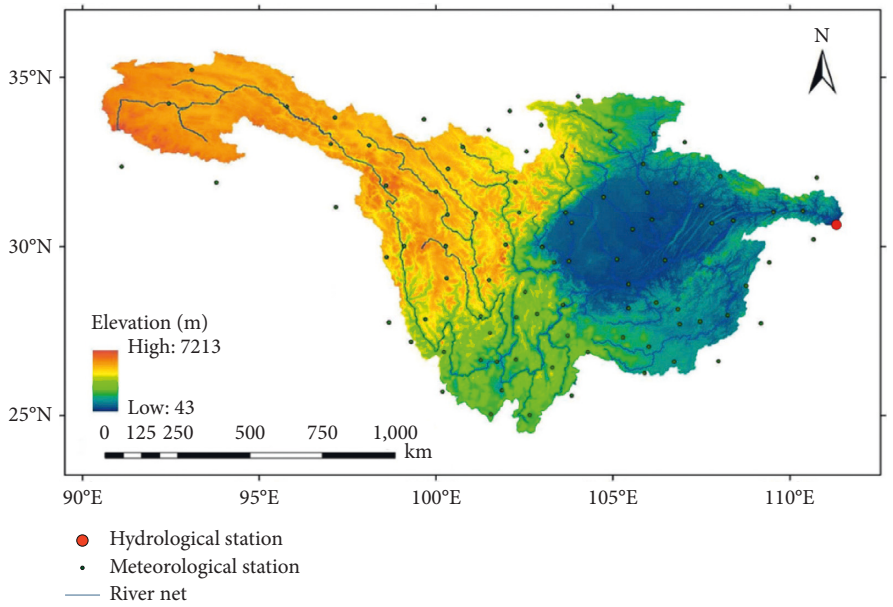

Figure 1: Elevation (in m) from DEM and locations of the meteorological stations and hydrological station in the Upper Yangtze River Basin (above the Yichang station).

Table 1: Information on eight global-coupled climate models.

Model name	Modeling center (or group)	Resolution (lat × lon)
bcc-csm1-1	Beijing Climate Center, China Meteorological Administration, China	2.8 × 2.8°
CanESM2	Canadian Centre for Climate Modeling and Analysis	2.8 × 2.8°
CCSM4	National Center for Atmospheric Research	1.25 × 0.9°
CSIRO-Mk3-6-0	Commonwealth Scientific and Industrial Research Organization in collaboration with Queensland Climate Change Centre of Excellence	1.875 × 1.875°
GISS-E2-R	National Aeronautics and Space Administration	2.5 × 2°
MRI-CGCM3	Meteorological Research Institute	1.125 × 1.125°
MPI-ESM-LR	Max Planck Institute for Meteorology	1.875 × 1.875°
NorESM1-M	Norwegian Climate Centre	2.5 × 1.875°

emission scenarios. Based on the time series of observational data from available stations and the CMIP5 projection period, we interpolate the data for the historical period of 1961–2005 and the future projection period of 2006–2099. The daily outputs of the eight GCMs were bias corrected to the 0.5 × 0.5° grid by using the EDCDF method and the observational data over the UYRB.

2.2. Methods. To analyze the future changes in the variability of hydrological regimes with climate change, eight bias-corrected GCMs outputs are used to force the VIC model to project the changes in extreme and average flows. We select 1961–1990 as the baseline period following the requirement of the World Meteorological Organization of using periods of at least 30 years for climate analysis. Furthermore, under the RCP4.5 and RCP8.5 scenarios, we divide the future period into three subperiods: 2010–2039 (near term), 2040–2069 (middle term), and 2070–2099 (long term). A multimodel ensemble (MME) is used to analyze the projected changes of hydrological regimes. Three hydrological regimes corresponding to the long-term availability of river discharge (MAR: mean annual runoff) and extreme flow (high flow Q_5: exceeded 5% of the time; and low flow Q_{95}: exceeded 95% of the time within a year) are selected. For each model, the MAR, Q_5, and Q_{95} of each year are calculated from the daily discharge simulation, resulting in 30 values for a 30-year period.

2.2.1. EDCDF Method. The EDCDF method developed by Li et al. [22] applies a quantile-based mapping of the CDFs between both the historic and projection period and matches the climatic fields in the future projection period. For temperature, this method uses a four-parameter beta function to fit the temperature fields, and the projection period is bias corrected with the following equation:

$$x_{\mathrm{m-p\_adjust}} = x_{\mathrm{m-p}} + F^{-1}_{\mathrm{o-c}}\left(F_{\mathrm{m-p}}\left(x_{\mathrm{m-p}}\right)\right) - F^{-1}_{\mathrm{m-c}}\left(F_{\mathrm{m-p}}\left(x_{\mathrm{m-p}}\right)\right), \quad (1)$$

where x is a climatic variable, $F^{-1}_{\mathrm{o-c}}$ is the quantile function corresponding to observation (o) for a historic training period (c), $F_{\mathrm{m-c}}$ is the PDF of the model-simulated fields (m) for a historic training period, and p is the future projection climate fields.

For precipitation, a two-parameter gamma distribution is used for the portion of a given time series with precipitation. The projected precipitation is bias corrected with the following equation:

$$x_{\mathrm{m-p\_adjust}} = x_{\mathrm{m-p}} \frac{F_{\mathrm{o-c}}^{-1}\left(F_{\mathrm{m-p}}\left(x_{\mathrm{m-p}}\right)\right)}{F_{\mathrm{m-c}}^{-1}\left(F_{\mathrm{m-p}}\left(x_{\mathrm{m-p}}\right)\right)}. \quad (2)$$

In the EDCDF method, the parametric distributions fit both the temperature and precipitation fields at each grid point and the distribution range parameters were taken as the extreme values from the data extended by half of one standard deviation of each grid cell. More details on this method are presented in Li et al. [22] and Yang et al. [26].

2.2.2. VIC Model. The VIC hydrological model developed by the University of Washington [29] is widely used for hydrological simulations, and it has a strong physical basis and a more realistic representation of hydrological processes [9]. The VIC model considers the dynamic variations in both the water and energy balances according to the subgrid heterogeneity represented by soil moisture storage, evaporation, and runoff generation [29–31]. This model uses the variable infiltration curve to account for the spatial heterogeneity of runoff generation. Vegetation is described by the leaf area index (LAI), canopy resistance, and the relative proportion of roots in soil. Vertical water movement occurs within discrete soil layers through diffusion, and base flow is modeled from a lower soil moisture zone as a nonlinear recession. For the three soil layers, the top layer can quickly respond to rainfall via evapotranspiration. The second soil layer regulates infiltration and excess runoff and controls the quick flow component. The third layer controls the base flow generation. More details on the VIC-3L model are presented at the VIC website [29, 30].

2.2.3. Statistical Method. The multimodel ensemble (MME) average is calculated with equal weights and commonly used for reducing noise in the projections [25]. The performances of the raw CMIP5 models and bias-corrected outputs against the observations are measured using the mean difference (bias) and probability of extreme values of climate fields. The bias, coefficient of determination (R^2), and Nash–Sutcliffe coefficient of efficiency (*NSCE*) [32] are used to evaluate VIC model performance. NSCE is defined as follows:

$$\mathrm{NSCE} = 1 - \frac{\sum_{i=1}^{n}\left(Q_{\mathrm{sim}}(i) - Q_{\mathrm{obs}}(i)\right)^2}{\sum_{i=1}^{n}\left(Q_{\mathrm{obs}}(i) - \overline{Q}_{\mathrm{obs}}(i)\right)^2}, \quad (3)$$

where Q_{obs} is the mean of observed discharges, Q_{sim} is the modeled discharge, and $Q_{\mathrm{obs}}(i)$ is the observed discharge at time i.

2.2.4. Direct Variance Method. In this study, the direct variance method [33] is used to calculate the contribution ratio of precipitation and temperature to the runoff changes. The direct variance method for decomposition is as follows:

$$\sigma_{\mathrm{pr}}^2 = \left(R_{\mathrm{pr}} - R_{\mathrm{o}}\right)^2, \quad (4)$$

$$\sigma_{\mathrm{tas}}^2 = \left(R_{\mathrm{tas}} - R_{\mathrm{o}}\right)^2, \quad (5)$$

where R_{o} is the runoff of the baseline period (1961–1990), R_{pr} is the simulated runoff by using RCP scenario precipitation and other input parameters for the baseline period data, and R_{tas} is the same as R_{pr} but for temperature. The contribution ratios of precipitation (C_{pr}) and temperature (C_{tas}) to the runoff changes are measured as follows:

$$C_{\mathrm{pr}} = \frac{\sigma_{\mathrm{pr}}^2}{\left(\sigma_{\mathrm{pr}}^2 + \sigma_{\mathrm{tas}}^2\right)},$$
$$C_{\mathrm{tas}} = \frac{\sigma_{\mathrm{tas}}^2}{\left(\sigma_{\mathrm{pr}}^2 + \sigma_{\mathrm{tas}}^2\right)}, \quad (6)$$

where the contribution ratio is between 0% and 100%. The sum of the contributions of the two climatic factors is 100%.

3. Results

3.1. Performance of EDCDF Method. We compare the spatial distributions of the bias of the monthly precipitation and temperature to verify the performance of the downscaled model outputs against the observational data (Figure 2). The results show that the bias-corrected model can dramatically reduce the bias of monthly precipitation and temperature from the original models. The MME of the original GCMs overestimates the precipitation varies from 0 to 144 mm per month in most regions but underestimates it by approximately 0.2 mm per month on some pixels of most of the east parts of the study area. The EDCDF shows remarkable skill in reducing the bias of precipitation, reducing it by −0.6 mm to −0.4 mm per month. On the contrary, the EDCDF can also obviously reduce the bias of the original model-simulated temperature. For temperature, the bias varies from −0.08°C to 0.06°C after downscaling, while the value for the original MME varies from −14°C and 0°C. This finding indicates that the EDCDF has an excellent ability to reduce the bias of the original models over the study area.

In addition, we evaluate the uncertainty of the EDCDF method's bias-corrected climate fields by using the probability plots of the extreme values of the monthly precipitation and temperature from the model simulations and observations at the 95 percent confidence level (Figures 3 and 4). In general, the EDCDF method has a strong ability to capture the precipitation and temperature distribution in the study area. However, a degree of uncertainty remains in the extreme precipitation values above the 0.9 probability level and under the 0.1 probability level compared to the observations. The EDCDF-downscaled models underestimate the extreme precipitation values in cases where the monthly precipitation is more than 140 mm per month and overestimate them in cases where the monthly precipitation is less than 10 mm per month. In the case of bias-corrected temperature, extreme values are more easily captured than

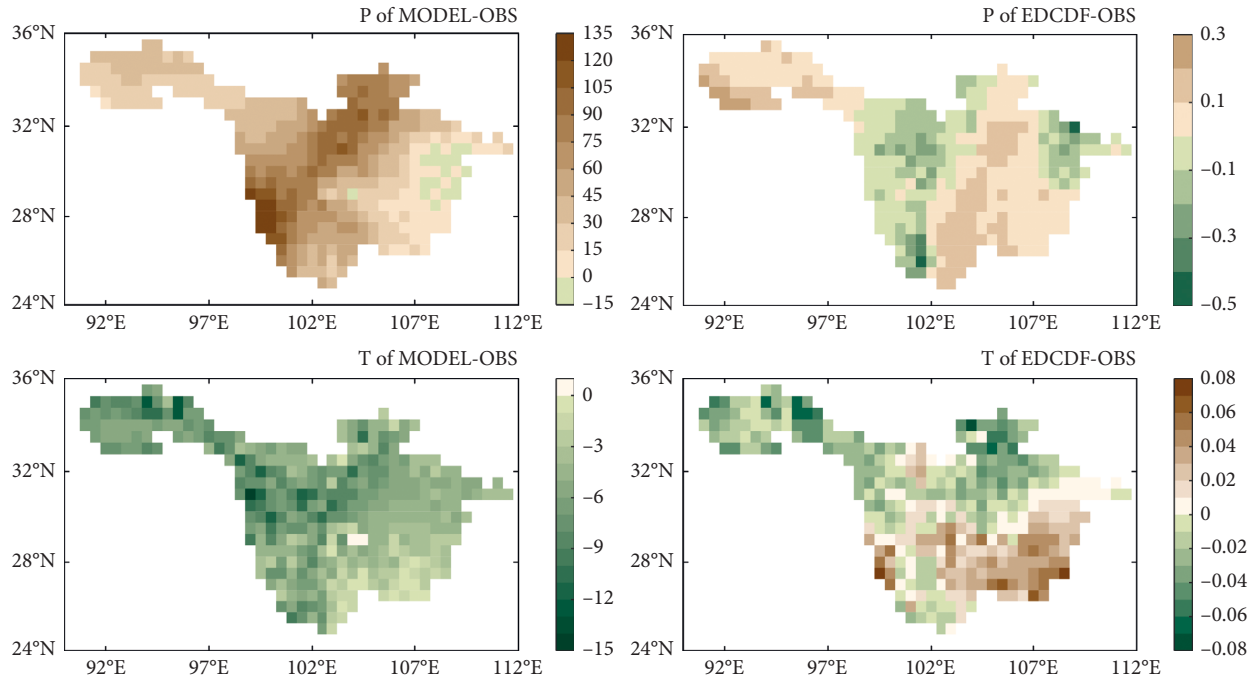

Figure 2: Spatial distribution of the bias of the original MME (MODEL-OBS) and EDCDF-downscaled MME (EDCDF-OBS) for the monthly precipitation (mm) and temperature (°C).

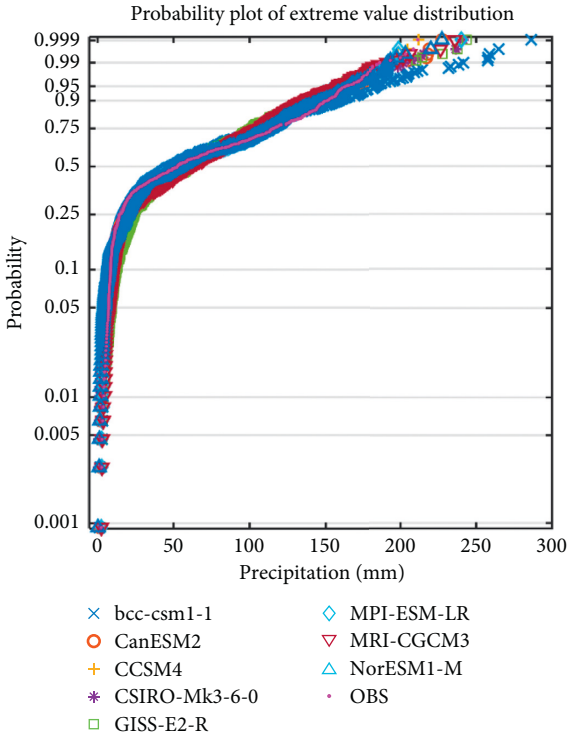

Figure 3: Probability plots of extreme values of monthly precipitation from observations and downscaled models from 1961 to 2005 in the UYRB.

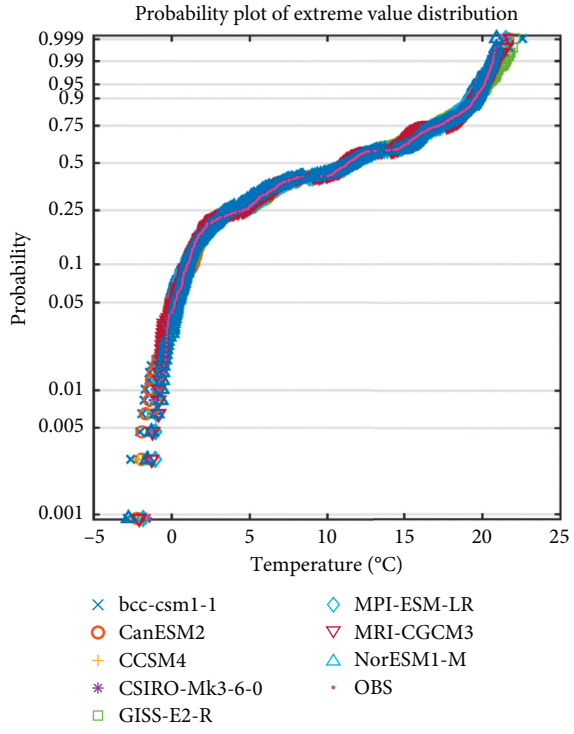

Figure 4: Probability plots of extreme values of monthly temperature from observations and downscaled models from 1961 to 2005 in the UYRB.

they are for precipitation. Meanwhile, the bias-corrected monthly temperatures show significant agreement with the observations within the ranges of the 0.1 to 0.90 probability level. The bias-corrected models show a pattern of underestimation and a colder pattern when the monthly temperature is below 1°C or above 19°C.

The aforementioned analyses show that bias correction is an important process during the statistical downscaling of

the GCMs in regional or local climate studies. The bias-corrected data of this study can be used for further studies of climatic impact and adaptation. In the following analyses, projections from eight GCMs ensemble are built using the arithmetic mean for 30-year future time slices (2010–2039, 2040–2069, and 2070–2099) under the RCP4.5 and RCP8.5 emission scenarios. Furthermore, the changes in VIC model-simulated hydrological variables are calculated by comparing the MME outputs for the three given subperiods with that of the baseline period (1961–1990).

3.2. Calibration and Validation of the VIC Model. The daily discharge observed at the Yichang station is used for model calibration and validation. According to the time-series discharge records of the Yichang hydrological station observations, the period of 1961–1970 is used for calibration, and the period of 1971–1990 is used for validation. The seven sensitive soil parameters (i, d_1, d_2, d_3, D_s, D_{smax}, and W_s) are calibrated using the NSCE and bias of the agreement between the simulated and observed hydrographs [34]. The specific meanings, ranges, and best fit values of the parameters are listed in Table 2. Finally, the validation process (1974–1987) is performed using the parameter set for the calibration period.

Figure 5 presents the calibration and validation results found using the daily discharge at the Yichang station. The NSCEs of the daily discharge used for calibration and validation are 0.708 and 0.797, respectively. The biases are −0.293 and −0.266 for the calibration and validation results, respectively. The R^2 values of the observation and simulation daily discharge are 0.889 and 0.934 for calibration and validation, respectively. The statistical analyses of the calibration and validation indicate that the model performed well in the daily discharge simulations. In the future period, we assume that the parameters used in the VIC model will not change with future climate changes, and the same parameters can be used for the hydrological simulations from 2006 to 2099 in the UYRB.

3.3. Projected Changes of Precipitation and Temperature. Table 3 shows the change ratios of annual precipitation and temperature from the MME of the eight CMIP5 models in the near, middle, and long terms for RCP4.5 and RCP8.5. The UYRB exhibits large intermodel and interannual variability in both temperature and precipitation for the two RCPs. Under both RCPs, similar patterns of annual precipitation are projected, and a decreasing trend is projected in the near term, whereas increasing ones are projected over the middle and long terms. On the contrary, the two RCPs show different magnitudes of changes. In the near and middle terms, the two RCPs project similar magnitudes of change of the annual precipitation, showing decreases of less than 1% and increases of more than 3%. In the long term, both RCPs project a relatively greater increase against the baseline period, while RCP8.5 projects a greater increase (9.28%) than RCP4.5 (7.41%). In the future, the two RCPs are projected to show similar rising trends of the annual temperature, although the magnitudes of the changes are greater under RCP8.5 than under RCP4.5. The greatest warming, 4.88°C, is projected in the long term under RCP8.5.

Table 2: Most sensitive parameters related to the UYRB, their description, the range used for the autocalibration, and the best fit value.

Parameter	Physical meaning	Unit	Range	Best fit value
i	Infiltration curve parameter	N/A	0–10	9
d_1	Thickness of the top thin soil moisture layer	m	0.05–0.2	0.05
d_2	Thickness of the middle soil moisture layer	m	0.5–0.95	0.52
d_3	Thickness of the lower soil moisture layer	m	1.44–2.1	1.6
D_s	Fraction of D_{smax} where nonlinear base flow begins	Fraction	0–1.0	0.75
D_{smax}	Maximum velocity of base flow	mm/day	0–30	7.5
W_s	Fraction of maximum soil moisture where nonlinear base flow occurs	Fraction	0–1	0.5

Table 4 presents the relative changes of monthly precipitation and temperature in summer and winter for the three future subperiods. The results show that the precipitation and temperature are projected to have the same change trends under the two RCPs, but a decreasing tendency in precipitation is observed in the near term under RCP8.5. Under the RCP4.5 scenario, the monthly precipitation in summer (June, July, and August) increases by between 0.20% and 6.90%, the greatest increase is projected to occur in the long term, and the smallest increase is projected in the near term. The RCP8.5 scenario shows variable trends in precipitation, with a decrease of −0.77% in the near term and increases of 3.23% and 8.02% in the middle and long terms, respectively. Both RCPs project increased precipitation in winter (December, January, and February) in the future. The change ratio of precipitation in the long term is larger than that of the middle and near terms. Similar to the RCP4.5 scenario, RCP8.5 also projects increased precipitation in winter, but it shows a wider potential range (2.47–20.29%) from the near term to the long term.

The projected monthly temperature under the two RCPs shows significant upward trends in summer and winter in the three future subperiods, but the ranges of the changes are narrower under RCP4.5. In addition, the magnitude of the temperature change is projected to undergo the greatest increase in summer in the long term. Under RCP8.5, the temperature in winter increases by 1.41°C relative to the baseline value in the near term and by 5.14°C in the long term. Note that the magnitude of the increase in temperature during winter is greater than that in summer in the near, middle, and long terms under both scenarios.

3.4. Projected Changes of Hydrological Regimes. The relative mean changes of Q_5, Q_{95}, and MAR under two RCPs in the future are presented in Figure 6. Under both RCPs, decreases of

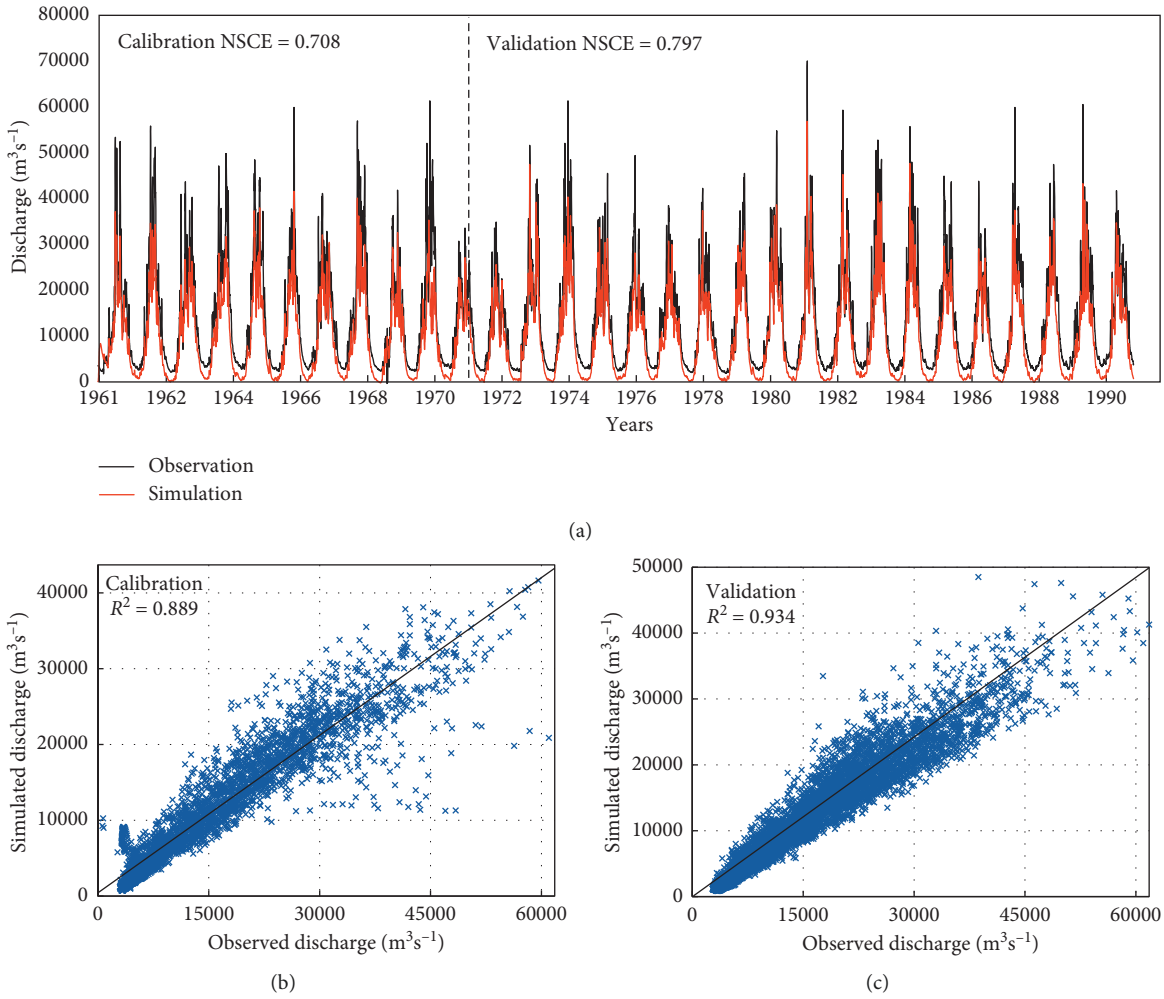

Figure 5: Nash–Sutcliffe coefficient of efficiency (a) and deterministic coefficients (b, c) of the observed and simulated daily discharge during calibration (1961–1970) and validation (1971–1990) periods in the UYRB.

Table 3: Change ratios of the annual precipitation and temperature in the near term, middle term, and long term from the MME in the UYRB.

	Precipitation (%)		Temperature (°C)	
	RCP4.5	RCP8.5	RCP4.5	RCP8.5
2010–2039	−0.43	−0.77	1.28	1.35
2040–2069	3.49	3.77	2.28	3.05
2070–2099	7.41	9.28	2.85	4.88

Table 4: Change ratios of precipitation and temperature during summer and winter in the near term, middle term, and long term from the MME in the UYRB.

	Precipitation (%)				Temperature (°C)			
	Summer		Winter		Summer		Winter	
	RCP4.5	RCP8.5	RCP4.5	RCP8.5	RCP4.5	RCP8.5	RCP4.5	RCP8.5
2010–2039	0.20	-0.77	1.83	2.47	1.25	1.33	1.36	1.41
2040–2069	3.41	3.23	9.60	11.33	2.21	2.92	2.43	3.26
2070–2099	6.90	8.02	18.05	20.29	2.71	4.69	3.03	5.14

Q_5, Q_{95}, and MAR are projected in all three future subperiods, but the distribution of decreasing median values is generally wider under RCP8.5 than RCP4.5 in the middle and long terms. Furthermore, the distribution of Q_{95} values in the near term is much larger under RCP4.5 than under RCP8.5. In the middle term, the decrease in MAR (−7.84%) under RCP8.5 is

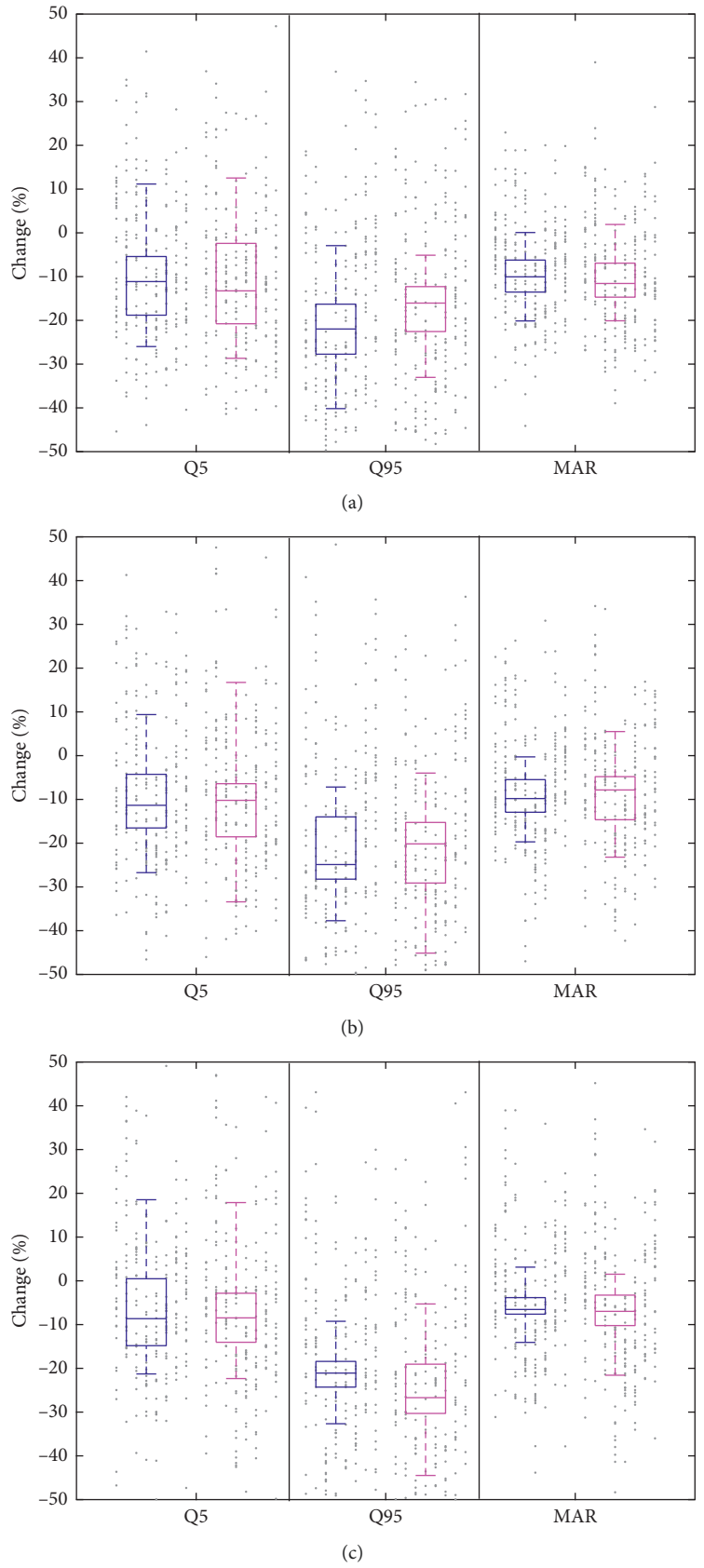

Figure 6: Change (%; vertical axis) of Q_5 (high flow), Q_{95} (low flow), and MAR for RCP4.5 (blue) and RCP8.5 (pink). The box-whiskers show the 10^{th}, 25^{th}, 50^{th}, 75^{th}, and 90^{th} percentiles of the distributions of changes of the three hydrological indicators (high flow (Q_5), low flow (Q_{95}), and MAR) during the (a) near, (b) middle, and (c) long terms. The gray points denote the change values of every year from each model.

smaller than that under RCP4.5 (−9.81%). The greatest decreases of MAR and Q_5 are projected to occur in the near term under RCP8.5, whereas the greatest decrease of Q_{95} is projected to occur in the long term under the same RCP. The Q_5 presents considerably greater decreases under RCP4.5 than RCP8.5 in the long term. Q_{95} decreases by a much greater magnitude and varies from −16.05% to 26.70% under RCP8.5, which is in contrast to the changes in MAR and Q_5. Additionally, the relative changes of Q_{95} in the near and middle terms under RCP4.5 are greater than those under RCP8.5.

To evaluate the relative changes of Q_5 and Q_{95} over the whole UYRB, we statistically evaluate the magnitude of their changes in summer and winter for the three subperiods (Table 5). Under both RCPs, the relative changes of Q_5 are highly consistent for the three future subperiods and show decreases in the near and middle terms but increases in the long term. Q_5 is projected to undergo a greater decrease (−2.82%) and increase (1.79%) under RCP8.5 than RCP4.5 in the near and long terms. Notably, Q_5 decreases under both RCPs with similar temperature trends, although summer precipitation increases slightly (0.20%) under RCP4.5 and decreases (−0.77%) under RCP8.5 in the near term. Under both RCP4.5 and RCP8.5, similar decreasing trends of Q_{95} in winter are projected for the three future subperiods. In the long term, RCP4.5 and RCP8.5 project decreases of Q_{95} of −17.34% and −26.25%, respectively.

The spatial patterns of the projected changes in Q_5 (high flow) in summer for the three future subperiods under RCP4.5 and RCP8.5 are shown in Figure 7. The results show that the spatial patterns of the relative changes in Q_5 are similar under the two RCPS during the three future subperiods. Under RCP8.5, the decreasing trend of Q_5 is observed in more than half of the whole basin (varying from 55.86% to 68.03%) for the near and middle terms. On the contrary, the area ratio of the decreasing trend in Q_5 reduces to 48.77% and 44.96% in the long term under RCP4.5 and RCP8.5, respectively. Specifically, the largest increase in Q_5 is projected to occur in the western upstream region of the basin, whereas the largest decrease is projected to occur in the northeastern parts of the basin. Although the spatial pattern of Q_5 is partially consistent for the two RCPs, the decreasing trends of Q_5 will occur in more regions for RCP8.5 than RCP4.5. Along the eastern border of the basin, Q_5 shows a positive tendency for RCP8.5 but a negative tendency for RCP4.5.

The spatial distribution of the changes in Q_{95} (low flow) shows that RCP4.5 and RCP8.5 project similar spatial patterns of Q_{95} changes during winter (Figure 8). Q_{95} decreases over 75.20% of the whole basin during the near term under RCP4.5, which is a larger area than that of RCP8.5. The areas with decreasing changes tendency in Q_{95} under RCP8.5 in the middle and long terms enlarge to 77.93% and 88.83% of the whole basin, respectively. In the near term, Q_{95} increases in some parts of the upstream region and decreases in most other parts of the basin which are projected under the two RCPs.

3.5. Influence of Precipitation and Temperature on Hydrological Regimes. Both precipitation and temperature have an influence on runoff. To evaluate the influence of climate fields on hydrological regimes, we analyze the contribution ratios of precipitation and temperature to the three hydrological regimes under the two RCPs (Figure 9). The results show that increases in temperature have a significant influence (more than 95%) on changes in Q_5 and MAR while precipitation plays a tiny role for the two RCPs in the near and middle terms. However, the contribution of precipitation to the Q_5 has increased by 20% for the long term. Both precipitation and temperature have almost equal contributions to Q_{95}, but the ratio of temperature (more than 53%) is slightly higher than that of precipitation under both RCPs in the three future subperiods. This finding demonstrates that the effect of temperature on hydrological regimes is more significant than that of precipitation in the study area, which is similar to the results found by Etter et al. [35] and Yu et al. [36].

We assume that the decreases in all hydrological regimes are driven by a remarkable increase in temperature, which leads to an increase in evaporation, and the slightly smaller increases in precipitation projected in the two scenarios. Furthermore, the decreases in Q_{95} for the near, middle, and long terms are greater than those in MAR and Q_5, which indicates that drought risk will increase in the future over the UYRB. This result is confirmed by the research of Lu et al. [37], which states that the regional drought could become more severely prolonged and frequent in the future in this region according to the Soil Moisture Anomaly Percentage Index. Dai et al. [2] and Birkinshaw et al. [1] found that higher temperatures coupled with greater evapotranspiration will lead to a decrease in discharge and drought risks.

Table 5: Watershed average with the change (%; vertical axis) in Q_5 during summer and change in Q_{95} during winter for RCP4.5 and RCP8.5 in the near term, middle term, and long term from the MME in the UYRB.

	Q_5 in summer (%)		Q_{95} in winter (%)	
	RCP4.5	RCP8.5	RCP4.5	RCP8.5
2010–2039	−1.28	−2.82	−5.68	−2.28
2040–2069	−0.98	−0.08	−10.50	−12.77
2070–2099	1.40	1.79	−17.34	−26.25

4. Discussion

We use the downscaled and bias-corrected outputs of eight GCMs to force the VIC model and evaluated the effects of climate change on hydrological regimes over the UYRB. Although this is a widely used and very helpful method for climate change studies, both GCMs and hydrological model simulations have many sources of uncertainty, e.g., in the predictors of GCMs and the parameters of the hydrological model. In this study, we use only those meteorological stations with observational data to bias correct the outputs of the GCMs without considering the uncertainties of the GCMs. In addition, we use the multimodel arithmetic average ensemble to analyze the climate changes and simulate river discharge. This widely used method has been considered appropriate for many studies [38, 39]. In this

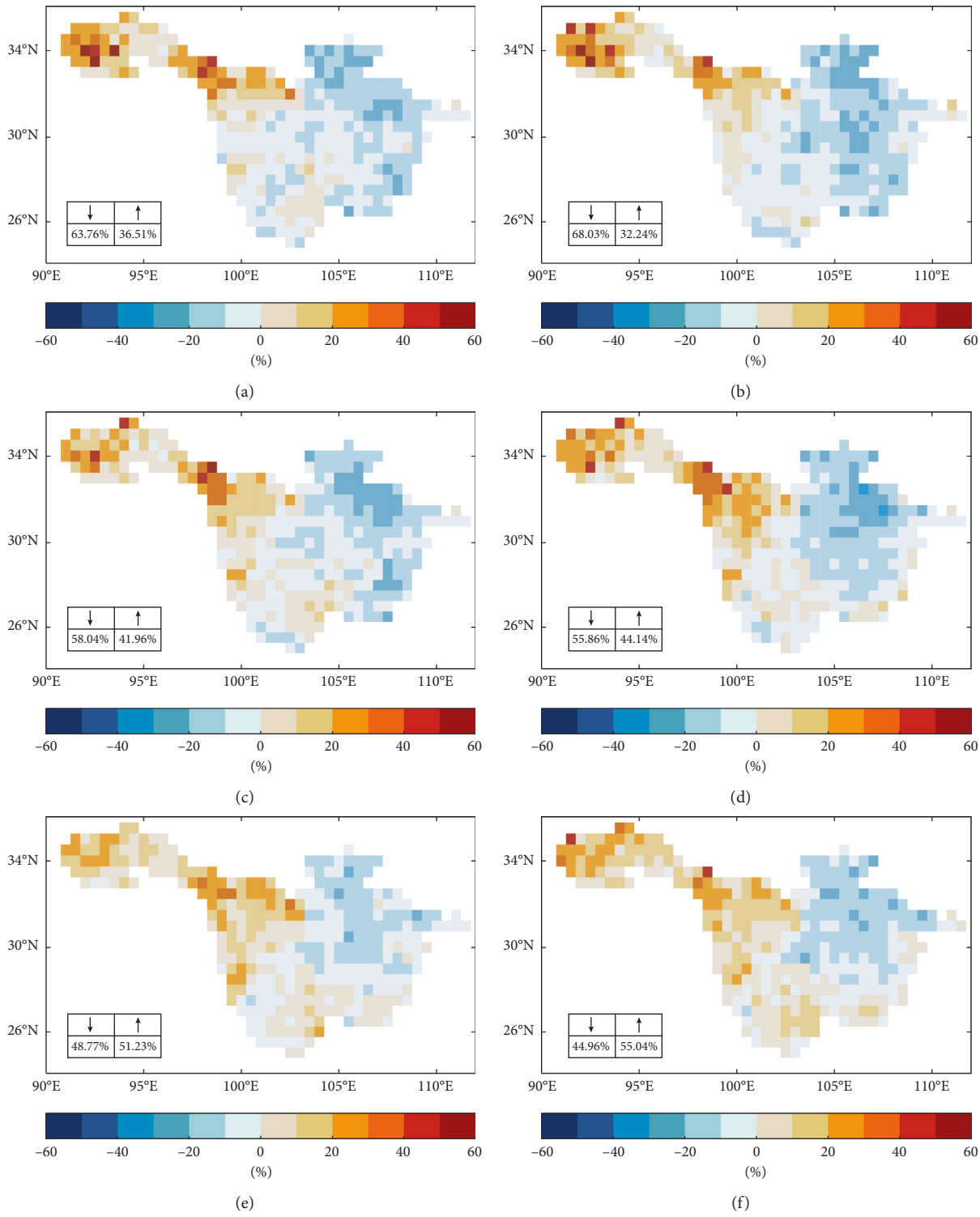

Figure 7: Relative changes (%; vertical axis) of Q_5 (high flow) in summer for RCP4.5 (a, c, e) and RCP8.5 (b, d, f) in the (a, b) near, (c, d) middle, and (e, f) long terms. Each figure is accompanied by a form that summarizes the percentage of the area that shows a changing magnitude. ↓ denotes a decrease, and ↑ denotes an increase.

method, the models with a poor simulation ability are averaged, and the simulation performance of each individual model is reduced. However, the optimal multimodel ensemble based on each model simulation performance requires further study.

The daily observed discharge values from the Yichang hydrological station are used to calibrate the parameters within the reasonable ranges of the VIC model, which mainly focuses on matching simulated and observed daily discharge. This process does not consider the uncertainties

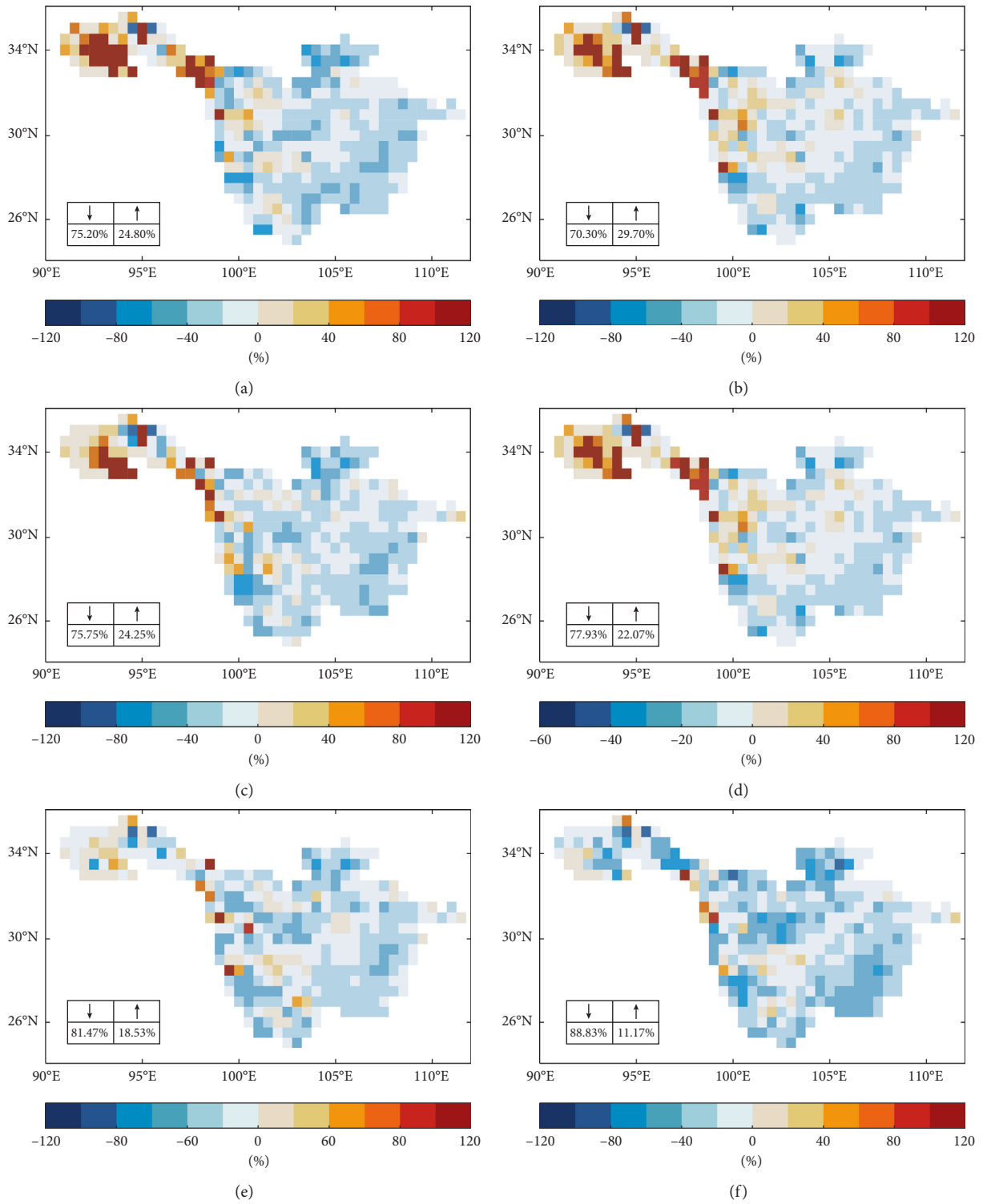

FIGURE 8: Relative changes (%; vertical axis) of Q_{95} (low flow) in winter for RCP4.5 (a, c, e) and RCP8.5 (b, d, f) in the (a, b) near, (c, d) middle, and (e, f) long terms. Each figure is accompanied by a form that summarizes the percentage of the area that shows a changing magnitude. ↓ denotes a decrease, and ↑ denotes an increase.

of the parameters and model structure. In this study, although the VIC model performs satisfactorily when simulating the hydrological processes over the UYRB, the VIC model underestimates Q_{95} during the calibration and validation periods. In future work, we can use additional hydrological models (such as land surface model) and additional parameter validation methods (such as observed soil moisture and evapotranspiration) to reduce the uncertainty and obtain a more accurate evaluation of the effects of climate change on hydrological regimes.

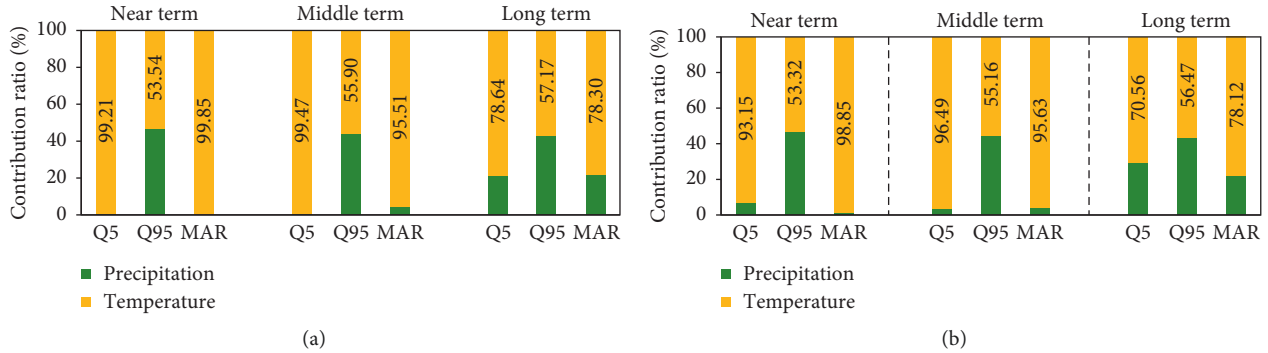

Figure 9: Contribution ratios of precipitation and temperature to Q_5, Q_{95}, and MAR for RCP4.5 (a) and RCP8.5 (b) in the near, middle, and long terms in UYRB.

Both precipitation and temperature influence the changes of Q_5, Q_{95}, and MAR. In this study, we use the direct variance method to quantify the contribution ratios of precipitation and temperature to the hydrological regimes. Under the projected increases in temperature, Q_5, Q_{95}, and MAR are projected to decrease, which will lead to increased drought risks in the future. Both climate change and human activities (e.g., human water consumption, irrigation, and reservoir) have effects on runoff, with population and economic changes showing an obviously increasing trend, especially after 2010 in the UYRB. Notably, the primary industry and secondary industry will increase and exceed the service industry, which requires more water resources. These facts indicate that the water resource demands in this region will increase to accommodate the growing population and economy. Therefore, the influences of human activities on water resources need further analysis.

5. Conclusions

We applied the EDCDF downscaling method to correct the bias of CMIP5 model outputs and evaluated their performances over the UYRB under two RCPs (RCP4.5 and RCP8.5). We used these tools together with the VIC model to project the potential changes of future MAR, Q_5, and Q_{95}. We considered eight GCM projections of the UYRB under RCP4.5 and RCP8.5 and examined the changes in precipitation and temperature between a historical period (1961–1990) and three future subperiods (2010–2039, 2040–2069, and 2070–2099). The results showed that the bias-corrected models perform well in terms of the spatiotemporal variability of precipitation and temperature over the UYRB. In the future, the temperature is projected to increase, while precipitation presents a more variable shift. Under the effects of temperature and precipitation changes, MAR, Q_5, and Q_{95} present a decreasing trend in the future. The values of both Q_5 and Q_{95} decrease by a greater degree than MAR. In particular, Q_{95} decreases in winter, with changes of −2.28% to −26.25% relative to the baseline value, as precipitation and temperature increase under the RCP8.5. Based on the results of the contribution ratios analysis, we found that the increase in temperature plays a decisive role in the reductions of Q_5 and annual average runoff while the increase in precipitation has limited effects under RCP4.5 and RCP8.5. The contribution of changes of temperature and precipitation to Q_{95} is nearly equivalent. These results indicate that droughts over the UYRB will increase considerably, with the MAR, Q_5, and Q_{95} showing unconspicuous decreasing trends. Therefore, a sustainable water resource management strategy must be designed to address the demands of economic development, food security, and ecosystem conservation when considering future climate change. Policymakers and water management personnel need to pay more attention to the probabilities of natural hazards in the Yangtze River.

Data Availability

In the manuscript, the daily precipitation and temperature data of 87 meteorological stations are from the National Meteorological Information Center (http://data.cma.cn/). The daily flows of the Yichang hydrological station (1961–2005) come from the Yangtze River Hydrology Bureau of China. The soil texture of the UYRB is derived from the 5 min Food and Agriculture Organization (FAO) dataset. Source of data is reliable.

Conflicts of Interest

The authors declare that there are no conflicts of interest.

Authors' Contributions

Xiaoli Yang and Liliang Ren conceived and designed this study. Mengru Zhang, Weifei Zheng, and Xiaohan Yu collected and processed the data. Xiaoli Yang and Yuqian Wang conducted the statistical work and analyzed the results. Yi Liu, Fei Yuan, and Shanhu Jiang provided many significant suggestions on the methodology and structure of the manuscript. All authors contributed to the preparation of this manuscript.

Acknowledgments

This research was financially supported by the National Key Research and Development Program under Grant no.

2016YFA0601504, which was approved by the Ministry of Science and Technology, the People's Republic of China. This research has also been funded by the National Natural Science Foundation of China (no. 51579066) and the Natural Science Foundation of Jiangsu Province (no. BK20150815).

References

[1] S. J. Birkinshaw, S. B. Guerreiro, A. Nicholson et al., "Climate change impacts on Yangtze River discharge at the three Gorges dam," *Hydrology and Earth System Sciences Discussions*, vol. 21, pp. 1–33, 2016.

[2] Z. J. Dai, A. Chu, J. Z. Du et al., "Assessment of extreme drought and human interference on baseflow of the Yangtze River," *Hydrological Processes*, vol. 24, no. 6, pp. 749–757, 2010.

[3] S. L. Yang, Z. Liu, S. B. Dai et al., "Temporal variations in water resources in the Yangtze River (Changjiang) over the Industrial Period based on reconstruction of missing monthly discharges," *Water Resources Research*, vol. 46, no. 10, 2010.

[4] S. Becker, M. Gemmer, and J. Tong, "Observed and interpolated precipitation trends and variability in the Yangtze catchment area," *Journal of Lake Sciences*, vol. 15, no. Z1, pp. 123–130, 2003.

[5] Y. Ding, G. Ren, G. Shi et al., "China's National Assessment Report on Climate Change (I): climate change in China and the future trend," *Advances in Climate Change Research*, vol. 1719, pp. 1–5, 2007.

[6] J. Tong, Z. Kundzewicz, and S. Buda, "Changes in monthly precipitation and flood hazard in the Yangtze River Basin, China," *International Journal of Climatology*, vol. 38, no. 11, 2008.

[7] K. Xu and J. D. Milliman, "Seasonal variations of sediment discharge from the Yangtze River before and after impoundment of the three Gorges dam," *Geomorphology*, vol. 104, no. 3-4, pp. 276–283, 2009.

[8] Q. Zhang, C.-Y. Xu, Z. Zhang, Y. D. Chen, C.-l. Liu, and H. Lin, "Spatial and temporal variability of precipitation maxima during 1960-2005 in the Yangtze River basin and possible association with large-scale circulation," *Journal of Hydrology*, vol. 353, no. 3-4, pp. 215–227, 2008.

[9] F. Su, L. Zhang, T. Ou et al., "Hydrological response to future climate changes for the major upstream river basins in the Tibetan Plateau," *Global and Planetary Change*, vol. 136, pp. 82–95, 2016.

[10] Z. Xiao, P. Shi, P. Jiang et al., "The spatiotemporal variations of runoff in the Yangtze River basin under climate change," *Advances in Meteorology*, vol. 2018, Article ID 5903451, 14 pages, 2018.

[11] H. Gu, Z. Yu, G. Wang et al., "Impact of climate change on hydrological extremes in the Yangtze River Basin, China," *Stochastic Environmental Research and Risk Assessment*, vol. 29, no. 3, pp. 693–707, 2014.

[12] M. Qian, X. Zheng-Hui, and Z. Lin-Na, "Variations of terrestrial water storage in the Yangtze River Basin under climate change scenarios," *Atmospheric and Oceanic Science Letters*, vol. 3, no. 6, pp. 293–298, 2015.

[13] S. Koirala, Y. Hirabayashi, R. Mahendran, and S. Kanae, "Global assessment of agreement among streamflow projections using CMIP5 model outputs," *Environmental Research Letters*, vol. 9, no. 6, 2014.

[14] IPCC, *Summary for Policymakers*, IPCC, Geneva, Switzerland, 2014.

[15] S. N. Gosling and N. W. Arnell, "A global assessment of the impact of climate change on water scarcity," *Climatic Change*, vol. 134, no. 3, pp. 371–385, 2013.

[16] N. W. Arnell and B. Lloyd-Hughes, "The global-scale impacts of climate change on water resources and flooding under new climate and socio-economic scenarios," *Climatic Change*, vol. 122, no. 1-2, pp. 127–140, 2013.

[17] M. A. Schnorbus and A. J. Cannon, "Statistical emulation of streamflow projections from a distributed hydrological model: Application to CMIP3 and CMIP5 climate projections for British Columbia," *Water Resources Research*, vol. 50, no. 11, pp. 8907–8926, 2014.

[18] H. Fowler and R. Wilby, "Beyond the downscaling comparison study," *International Journal of Climatology*, vol. 27, no. 12, pp. 1543–1545, 2007.

[19] L. E. Hay, R. L. Wilby, and G. H. Leavesley, "A comparison of delta change and downscaled GCM scenarios for three mountainous basins in the United States1," *JAWRA Journal of the American Water Resources Association*, vol. 36, no. 2, pp. 387–397, 2007.

[20] A. W. Wood, L. R. Leung, V. Sridhar, and D. P. Lettenmaier, "Hydrologic implications of dynamical and statistical approaches to downscaling climate model outputs," *Climatic Change*, vol. 62, no. 1–3, pp. 189–216, 2004.

[21] C. M. M. Goodess, C. Anagnostopoulou, A. Bárdossy et al., *An Intercomparison of Statistical Downscaling Methods for Europe and European Regions—Assessing Their Performance with Respect to Extreme Temperature and Precipitation Events*, Climatic Research Unit Research Publications, Norwich, UK, 2005.

[22] H. Li, J. Sheffield, and E. F. Wood, "Bias correction of monthly precipitation and temperature fields from Intergovernmental Panel on Climate Change AR4 models using equidistant quantile matching," *Journal of Geophysical Research*, vol. 115, no. D10, 2010.

[23] L. Wang and W. Chen, "A CMIP5 multimodel projection of future temperature, precipitation, and climatological drought in China," *International Journal of Climatology*, vol. 34, no. 6, pp. 2059–2078, 2013.

[24] S. Watanabe, S. Kanae, S. Seto et al., "Intercomparison of bias-correction methods for monthly temperature and precipitation simulated by multiple climate models," *Journal of Geophysical Research: Atmospheres*, vol. 117, no. D23, pp. 1–13, 2012.

[25] N. R. Aloysius, J. Sheffield, J. E. Saiers, H. Li, and E. F. Wood, "Evaluation of historical and future simulations of precipitation and temperature in central Africa from CMIP5 climate models," *Journal of Geophysical Research: Atmospheres*, vol. 121, no. 1, pp. 130–152, 2016.

[26] X. Yang, E. F. Wood, J. Sheffield et al., "Bias-correction of historical and future simulations of precipitation and temperature for China from CMIP5 models," *Journal of Hydrometeorology*, vol. 19, no. 3, pp. 609–623, 2018.

[27] J. A. Deckers and F. Nachtergaele, *World Reference Base for Soil Resources*, Food and Agriculture Organization, Vol. 84, Food and Agriculture Organization, Rome, Italy, 1998.

[28] M. C. Hansen, R. S. Defries, J. R. G. Townshend, and R. Sohlberg, "Global land cover classification at 1 km spatial resolution using a classification tree approach," *International Journal of Remote Sensing*, vol. 21, no. 6-7, 2000.

[29] X. Liang, D. P. Lettenmaier, E. F. Wood, and S. J. Burges, "A simple hydrologically based model of land surface water and energy fluxes for general circulation models," *Journal of Geophysical Research*, vol. 99, no. D7, pp. 14415–14428, 1994.

[30] X. Liang, E. F. Wood, and D. P. Lettenmaier, "Surface soil moisture parameterization of the VIC-2L model: evaluation and modification," *Global and Planetary Change*, vol. 13, no. 1-4, pp. 195–206, 1996.

[31] B. Nijssen, D. P. Lettenmaier, X. Liang, S. W. Wetzel, and E. F. Wood, "Streamflow simulation for continental-scale river basins," *Water Resources Research*, vol. 33, no. 4, pp. 711–724, 1997.

[32] J. E. Nash and J. V. Sutcliffe, "River flow forecasting through conceptual models part I—A discussion of principles," *Journal of Hydrology*, vol. 10, no. 3, pp. 282–290, 1970.

[33] F. Yuan, C. Zhao, Y. Jiang et al., "Evaluation on uncertainty sources in projecting hydrological changes over the Xijiang River basin in South China," *Journal of Hydrology*, vol. 554, pp. 434–450, 2017.

[34] Y. Liu, X. Yang, L. Ren, F. Yuan, S. Jiang, and M. Ma, "A new physically based self-calibrating palmer drought severity index and its performance evaluation," *Water Resources Management*, vol. 29, no. 13, pp. 4833–4847, 2015.

[35] S. Etter, N. Addor, M. Huss, and D. Finger, "Climate change impacts on future snow, ice and rain runoff in a Swiss mountain catchment using multi-dataset calibration," *Journal of Hydrology: Regional Studies*, vol. 13, pp. 222–239, 2017.

[36] Z. Yu, H. Gu, J. Wang, J. Xia, and B. Lu, "Effect of projected climate change on the hydrological regime of the Yangtze River Basin, China," *Stochastic Environmental Research and Risk Assessment*, vol. 32, no. 1, pp. 1–16, 2017.

[37] G. Lu, H. Wu, H. Xiao, H. He, and Z. Wu, "Impact of climate change on drought in the upstream Yangtze River region," *Water*, vol. 8, no. 12, p. 576, 2016.

[38] P. Mote, L. Brekke, P. B. Duffy, and E. Maurer, "Guidelines for constructing climate scenarios," *Eos, Transactions American Geophysical Union*, vol. 92, no. 31, pp. 257–264, 2011.

[39] H. M. Kim, P. J. Webster, and J. A. Curry, "Evaluation of short-term climate change prediction in multi-model CMIP5 decadal hindcasts," *Geophysical Research Letters*, vol. 39, no. 10, pp. 1–7, 2012.